CORROSION SCIENCE AND TECHNOLOGY, Vol.18, No.5(2019), pp.175~181
[Research Paper]
pISSN: 1598-6462 / eISSN: 2288-6524
DOI: https://doi.org/10.14773/cst.2019.18.5.175

Investigation of Pellet-Clad Mechanical Interaction in Failed Spent PWR Fuel

Yang Hong Jung† and Seung Je Baik

Korea Atomic Energy Research Institute, 111 Daedeok-daero, Yuseong-gu, 989-Bungil, Daejeon, 305-353, Republic of Korea

(Received September 18, 2019; Revised October 21, 2019; Accepted October 23, 2019)

A failed spent fuel rod with 53,000 MWd/tU from a nuclear power plant was characterized, and the fission products and oxygen layer in the pellet-clad mechanical interaction region were observed using an EPMA (Electron Probe Micro-Analyzer). A sound fuel rod burned under similar conditions was used to compare and analyze, the results of the failed fuel rod. In the failed fuel rod, the oxide layer represented 10 μm of the boundary of the cladding, and 35 μm of the region outside the cladding. By comparison, in the sound fuel rod, the oxide layer was 8 μm, observed in the cladding boundary region. The cladding inner surface corrosion and the resulting fuel-cladding bonding were investigated using an EPMA. Zirconium existed in the bonding layer of the (U, Zr)O compound beyond the pellet cladding interaction gap of 20 μm, and composition of UZr2O3 was observed in the failed fuel rod. This paper presents the results of the EPMA examination of a spent fuel specimen, and a technique to analyze fission products in the pellet-clad mechanical interaction region.

Keywords: *Pellet-clad mechanical interaction, A fission product, Hot-cell, Bonding layer*

1. Introduction

Zirconium alloy cladding is the first containment barrier for fission products. Due to water pressure, the cladding creeps down until contact with the pellet occurs after a few operating cycles. In the case of a power increase, this pellet-cladding mechanical interaction (PCMI) induces large stresses in the cladding, which can lead to fuel rod failure. Therefore, it is necessary to be able to prevent the occurrence of PCMI failure [1]. If a gap is initially present in the rod, a sufficiently large pellet strain is required to produce mechanical interaction with the cladding, which will take place particularly in regions next to the pellets ends [2]. The cladding may be either of the elastic or plastic types, and creep may have a significant effect over sufficiently long periods. Due to the low thermal conductivity of the fuel material (UO_2), quite a steep temperature gradient appears in the pellet. Considerably high temperatures are reached at the pellet center. Due to thermal expansion and to the absence of mechanical restraints at the top and bottom of the pellet, it experiences a non-uniform deformation known as hour glassing. The initially cylindrical pellet surface distorts, bending outwards, and the ends experience greater radial strain than the central belt [3].

In the case of a power increase, the thermal expansion of the pellet results in a rapid increase in pellet diameter accompanied by pellet crack opening. Moreover, at high power, gaseous fission products are created and stored in the fuel, causing an additional pellet diameter increase.

If the gap is already closed, this causes enhanced stresses in the cladding that might lead to cladding failure. Experimental observations have shown that the failure mechanism is most often stress-corrosion cracking (SCC), due to corrosive fission products such as iodine released within the fuel rod. “PCI failure” is usually defined as a cladding failure due to iodine-induced SCC in conditions of mechanical interaction. It is worth noting that another kind of failure mechanism during a power increase has been observed in highly hydride cladding, which is delayed hydride cracking (DHC) [4].

The noble gas xenon is distributed, and the general trend for release and redistribution is shown in the fuel-clad gap regions. X-ray microanalysis of xenon yields qualitative determinations of the unreleased fraction in irradiated fuels. The relative xenon intensities of predominantly intra-granular xenon can be calibrated by a fraction of the total xenon [5]. Zircaloy cladding is known to have a strong affinity for oxygen. The in-reactor corrosion of the cladding typically produces a thin outer layer of oxide

†Corresponding author: nyhjung@kaeri.re.kr

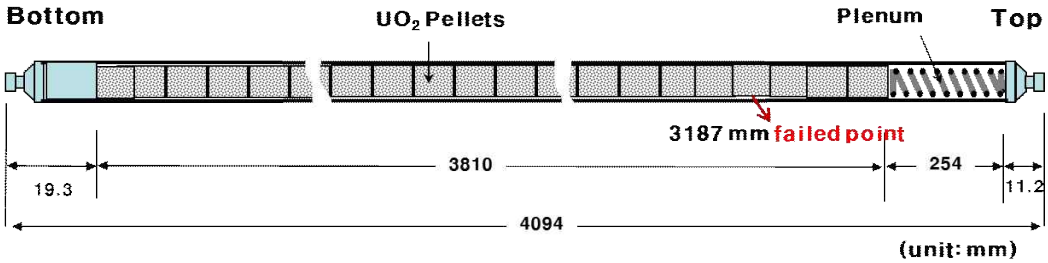

Fig. 1 Fuel rod design specification and damaged site location.

8 - 40 μm in thickness. During the reprocessing of spent fuel elements, the fuel rods are cut into pieces a few centimeters in length and the spent fuel content is dissolved in an acid solution. The remaining cladding hulls are contaminated with actinides and fission products [6]. The characterization of the hulls is of interest not only for the safety of waste disposal but also for the improvement of the processing process.

2. Experimental preparations

A thin diamond wheel was used to cut samples from a PWR failed spent fuel rod with 56,000 MWd/tU, that had been withdrawn from a nuclear power plant and cooled down for two years. In addition, a 53,750 MWd/tU burned sound fuel rod was cut with a diamond wheel for comparison with the results of the failed fuel specimen. The work for cutting and preparing the fuel rod specimens preceded in a hot cell space designed to enable the operation of highly radioactive materials [13].

The samples were embedded in epoxy resin and polished with diamond grinding disks of successively finer grain size, and finished with a diamond paste of 1 μm as the final stage. Before mounting each sample in the EPMA, the samples were coated with carbon to prevent charging. The carbon-coated specimens were mounted in a holder together with the X-ray standard. The standard specimen manufacturer is MAC and Registered Standard No is 11580. The EPMA was performed using a CAMECA SX-50R equipped with a two-wavelength dispersive X-ray spectrometer shielded with tungsten.

In the EPMA, the radiation activity allowed was up to 3.7×10^{10} Bq. The specimen holder as a part of the equipment was shielded from radiation leakage, and wavelength dispersive spectroscopy count windows containing lead and tungsten were used for the analysis of irradiated nuclear fuel [7].

The analysis was performed with a beam current of 50 nA at an accelerating voltage of 25 kV, in order to give a reasonable peak-to-background ratio for an active specimen. It was operated so that an electron beam was focused exactly at the center of the fuel-clad gap and crud layer. At the same time, tiny vibrations were excluded during measurement by turning off the stage motor while measuring. The electron beam was in fixed mode with 1 μm beam size.

The γ-activity was maintained within the tolerances specified above. Although a specimen has to be maintained at a sufficiently small size, its volume can be managed with a manipulator in a hot cell. After cutting the specimens into a manageable size with the manipulator, the specimens were hot- mounted with a conducting resin at 150 °C and 0.6 MPa. An overly thin specimen is apt to break during hot mounting, and thus a specimen was cut to about 5 mm of its depth at first, and finally a specimen of $2.5 \times 5 \times 1.5$ mm^3 was fabricated by repeating the mounting and cutting processes several times to decrease the radiation level by using a manipulator. The specimen was subsequently polished in a conventional manner with γ -monitoring until the activity was considered to be low enough to handle it.

To enhance the electric conductivity, silver paint (Leistsilver 2000 silver paint, TED PELLA, INC.) was brushed over the surface of the specimen. Precautions were taken to avoid any contamination of the SX-50R instrument. The mounted sample was cleaned with alcohol and held under a vacuum for 10 hours to ensure that no loose particles remained.

3. Results and discussion

The location of the failed fuel rod is shown in Fig. 1. The damaged area was found at a height of 3,187 mm from the bottom. In order to observe PCMI of the failed fuel rad, a drilling operation was performed to remove highly radioactive nuclear material as shown in Fig. 1. A schematic drawing of the sample preparation is shown in Fig. 2. Drilling and cutting devices capable of handling highly radioactive materials in a hot cell. In general, the process of preparing irradiated fuel specimens cuts the

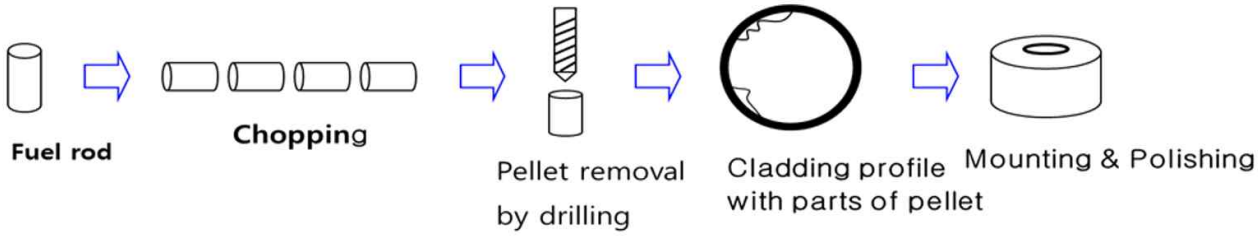

Fig. 2 Schematic of a sample cut off from a PWR fuel rod using a thin diamond wheel.

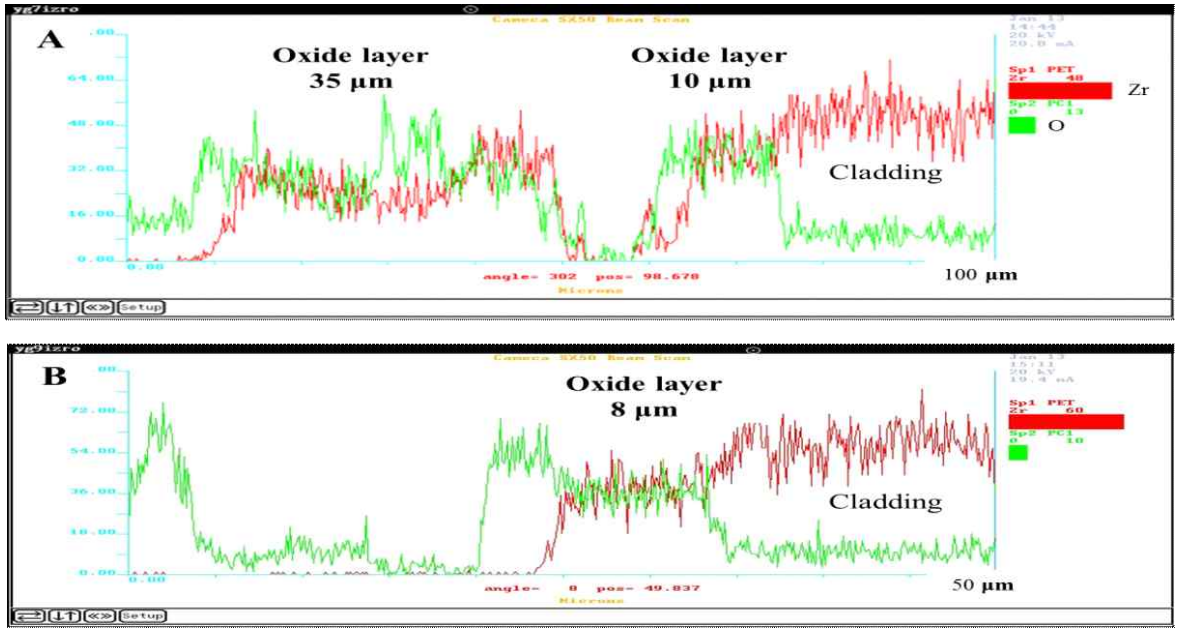

Fig. 3 Profiles of Zr, and O in the failed fuel(A) and sound fuel rod cladding PCMI region(B).

thickness of the pellet to about 2 mm in order to minimize the effects of high radiation on the operator and the EPMA equipment. The cut specimen is then mounted using a hot-mounting device installed in a hot cell. Sometimes, lowering the radiation dose of the prepared specimen is accomplished by splitting the mounted fuel specimen into two or four pieces.

Fig. 3 shows the PCMI region oxide layer profile of the failed fuel and normal fuel rod. The normal fuel rod specimen was extracted at a height of 2,957 mm from the bottom, which was similar to the failed fuel rod specimen location. The average design burn-up of the fuel rod was 53, 750 MWd/tU, having a burning history similar to that of the failed fuel rod. As shown in Fig. 3A, it can be seen that the oxide layer represents 10 μm of the boundary of the cladding, and 35 μm of the region outside the cladding area. In the profile of Zr and O in Fig. 3B, an oxide layer with a size of 8 μm is observed in the cladding boundary region. This result is in contrast to Fig. 3A [13].

Fig. 4 shows the SEM images and X-ray image mapping at the same positions as shown in the profile of Fig. 3A. In the SEM image of Fig. 4, there is a compound with a thick thickness of about 20 ~ 30 μm after the cladding and bound resin region. If a gap is initially present in the rod, a large pellet strain is required to produce mechanical interaction with the cladding, which will take place particularly in regions next to the pellets ends. The fuel rod acquires, in that case, the aspect of a cane. This compound is known to cause PCMI, if the pellet deformation is sufficiently large as a bonding phenomenon due to UO_2/Zircaloy interaction. This phenomenon was more thermodynamically unstable than the fuel, so chemical interaction between the fuel and the cladding may occur when the fuel rod was exposed to high temperature [8,9,13].

The X-ray image mapping of U, Zr, and O in Fig. 4 shows that the bonding layer thickness of (U, Zr)O was

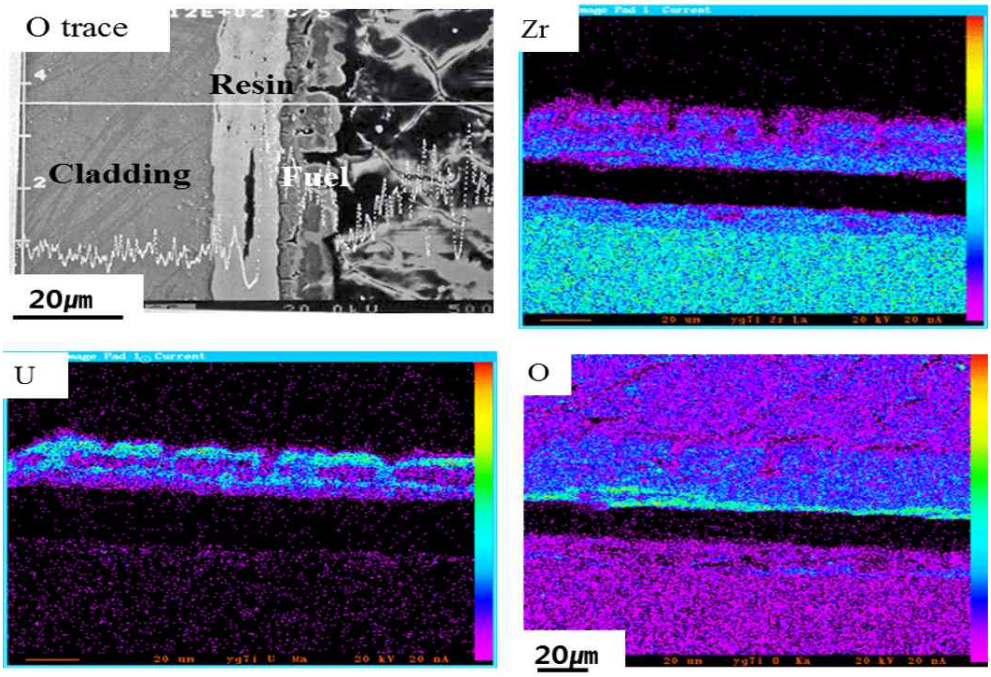

Fig. 4 SEM image of PCMI in the failed fuel rod and X-ray image mapping of O, Zr, and U.

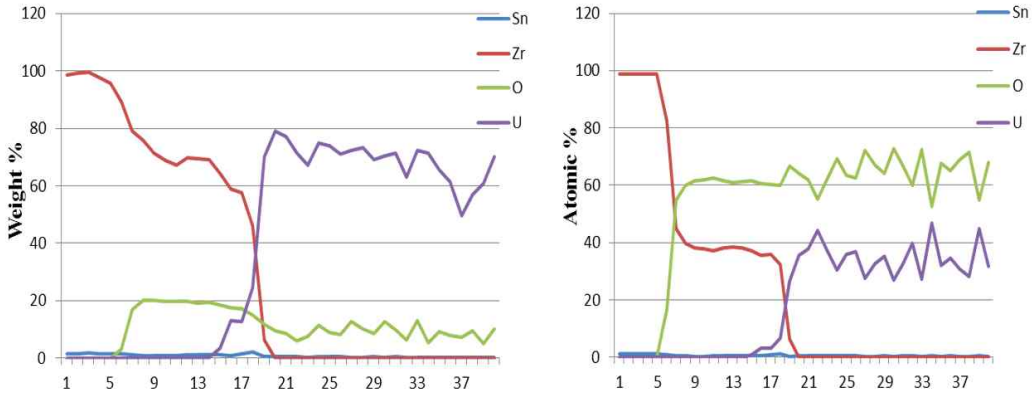

Fig. 5 Quantitative analysis of O, Zr, and U on inside cladding oxide and bonding layer (wt% & at.%).

estimated to be 20 ~ 30 μm. In Fig. 4, the gap between the cladding layer and the bonding layer was estimated to be about 20 μm. Uranium does not exist at the cladding interface at all. On the contrary, zirconium exists in the bonding layer of the (U, Zr)O compound beyond the PCI gap of 20 μm, and oxygen also shows a similar tendency to zirconium. In many papers related to PCMI, reference was often made to the bonding layer, but it was difficult to observe the SEM image of the cane phenomenon as shown in Fig. 4. This was observed only in failed nuclear fuel rods. This figure shows a large difference from the failed fuel rod, especially in the thickness of the oxide layer.

In the sound fuel rod, it can be seen that the uranium bonding layer exists not only in a thickness of several micrometers at the cladding interface but also in a constant band on both sides of the PCMI gap. Fig. 7 shows a fuel rod with above 50,000 MWd/tU burn-up, which has been burned for 1,400 days during three cycles. It is assumed that the uranium bonding layer was generated by the pellet-clad mechanical interaction due to the power bump during high-combustion for long periods.

Fig. 5 shows the results of quantitative analysis of the distribution of Zr, U, Sn and O. Table 1 shows the average of each element in 10 μm in the result of Fig. 5. Table 1 shows the ratio of Zr/O, and average values from 8 to 17 in the axial direction are shown in Fig. 5. In Table 1, Zr was 37.62 at.% and O was 61.22 at.%. Its chemical

Table 1 Chemical composition of Zr, U, and O in 10 μm, as shown in Fig. 5 (at.%)

El/Point		1	2	3	4	5	6	7	8	9	10	Ave.
Zr/O	Zr	39.69	38.17	37.76	37.09	38.06	38.55	38.12	37.27	35.71	35.78	37.62
	O	59.86	61.46	61.87	62.5	61.44	60.97	61.34	61.47	60.77	60.45	61.22
U/O	O	62.64	72.14	67.12	64.21	72.87	66.83	59.89	72.65	52.74	67.75	65.89
	U	36.89	27.54	32.54	35.31	26.83	32.76	39.67	27.06	46.78	31.91	33.73

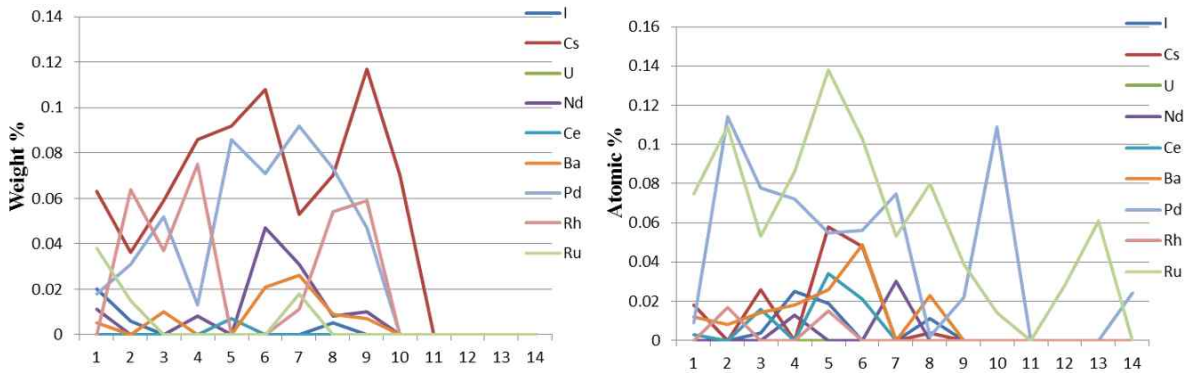

Fig. 6 Distributions of fission products profile in recoil layer region in the failed fuel rod (wt% & at.%).

formula can be written as ZRO_2. Table 1 show the result of the analysis point where the gap between the cladding layer and the bonding layer was very narrow. Unfortunately, in Fig. 4, the quantitative analysis of the entire region from cladding to the bonding layer representing the bamboo effect was not analyzed.

Some researchers have confirmed that Zr_2O, ZrO_2, Zr_2O_3, and so on sub-oxides are formed on the surface depending on the oxygen partial pressure supplied when oxidizing zirconium [10]. It is also known that even when Zircaloy-4 cladding was oxidized, low-oxidation oxides such as ZrO_2 and Zr_2O_3 are formed together with ZrO_2 [11,13].

The composition of U, Zr, and O in the bonding layer of Fig. 5 showed that the concentration of Zr was 33.28 wt%, U was 43.31 wt%, and O was 13.98 wt%. The total concentration measured in this region was 90.53 wt%. The weight ratio of this compound to atomic ratio is as follows: The concentration of U was 12.87 at.%, Zr was 25.76 at.%, and atomic ratio oxygen was 61.36 at.%. Its chemical formula can be written as UZr_2O_3.

As well known, it is difficult to measure the quantitative value of oxygen using an EPMA analyzer. The surface condition of the specimen, the composition of the specimen and the conductivity are obstacles to the accurate analysis of the quantitative value of oxygen.

Of course, the analysis of oxygen composition in spent fuel is also difficult. This means that it is not easy to analyze the exact composition because the conductivity of the fuel is much lower than that of common metals. The results in Table 1 indicate these data in order to prove that there is no error in the measurement of oxygen. In Table 1, the ratio of 10-point average oxygen was 65.89 at.% and U was 33.73 at.%. Its chemical formula can be written as UO_2. In other words, it was confirmed that the measurement value of oxygen shown in Table 1 was reliable.

The chemistry of the alkali metal cesium in irradiated oxide fuels is of high interest because these fission products react with the fuel, with cladding components, and with other fission products leading to pin swelling and cladding corrosion at higher oxygen potentials. Most of the redistributions of the fission product nuclide are measured by classical methods of micro-sampling.

The amount of fission products present in the hull region is known to be negligible. Therefore, most of the production amount is indicated by the counting amount of the characteristic X-ray.

However, in this test, quantitative analysis of fission product was performed using an EPMA instrument and the result is shown in Fig. 6 and Fig. 8. The conditions of the apparatus for quantitatively analyzing the fission product were 20 kV, 100 nA and the counting time was 50 ms. This is the general method used when analyzing elements with trace amounts of composition. Attention was also paid to the selection of standard specimens.

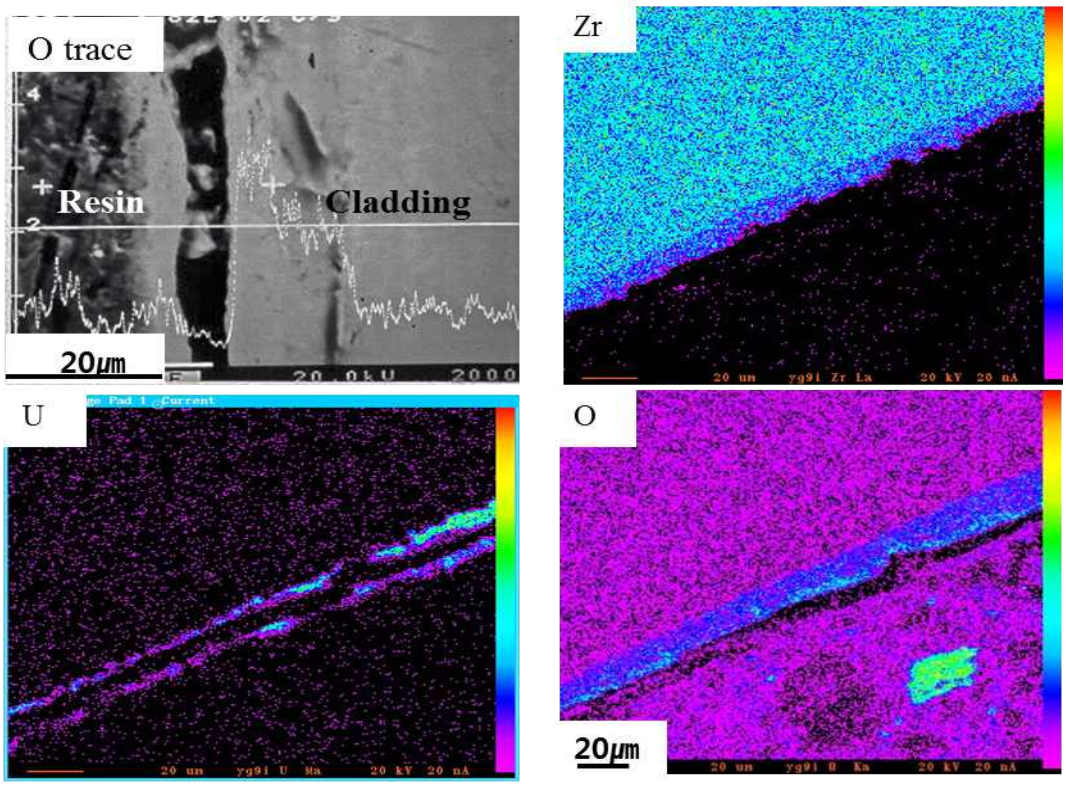

Fig. 7 SEM image of PCMI in the sound fuel rod cladding and X-ray image mapping of O, Zr, and U.

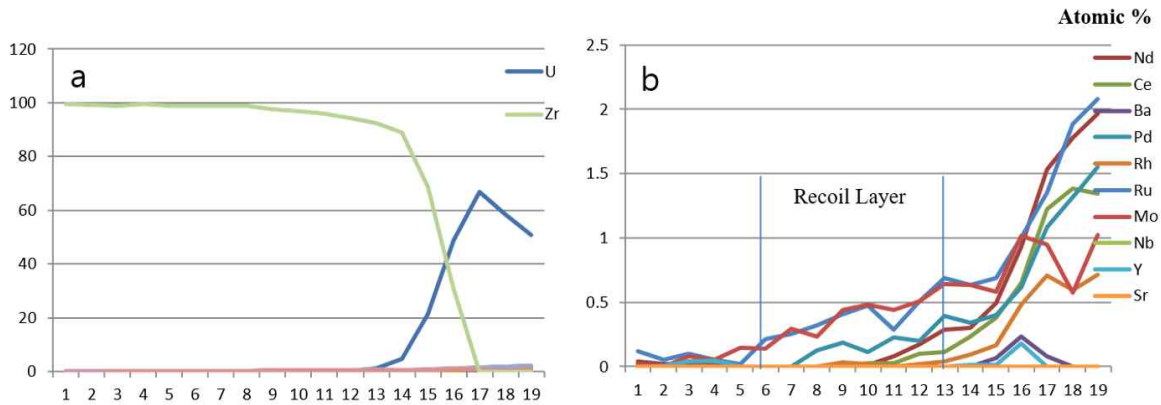

Fig. 8 Distributions of fission products profile in recoil layer region in the sound fuel rod using EPMA (a. U and Zr profile. b. Recoil layer region).

The analysis direction was from cladding to fuel area. The distance of the analysis position interval was 1 μm, and quantitative analysis is performed for a total of 20 μm area. In Fig. 8, analysis points 1 to 13 are the distribution of fission products in the cladding. It can be seen that the trend is toward a gradual increase with progress toward nuclear fuel.

The outer surface of the Zircaloy hulls is large, with closely associated areas of contamination. On the fuel side, there are also some residues of insufficiently rinsed or un-dissolved fuel, corrosion products of the ZrO_2 layer by recoil processes during fission, and by thermal diffusion [12].

The recoil layer region can be set roughly from 5 to 13 in Fig. 8, and the concentration of fission products is rapidly increased in the region of 14 μm or more in distance. As comparative data on this result, reference material, which analyzed the recoil layer using Secondary Ion Mass Spectroscopy (SIMS) were studied [5]. The spent fuel used in the reference was 30,000 MWd/tU

burn-up and 30 years' fuel element discharged. The reference and recoil layer areas have different burn-up, while the recoil layer area close to 12 μm for both samples. These results may vary depending on the setting of the test site and the recoil layer area. In this experiment, the significance of the analysis is that it is possible to measure the fission distribution of the recoil layer region using SIMS and EPMA instruments.

Thus, the results of the analysis of fission products using an EPMA demonstrate that the results are close to SIMS. With this test, we will continue to analyze the Zircaloy fission recoil analysis using an EPMA analyzer. Knowledge of the residual activities and of their fixation processes on the hulls allows better modeling of radionuclide release in disposal safety analysis and better elimination of these radio-nuclides during reprocessing through adapted fuel dissolution and hull rinsing.

4. Conclusion

A failed spent fuel rod with 53,000 MWd/tU and their fission products and oxygen layer in the PCMI region were observed using an EPMA. A sound fuel rod was used for comparative analysis of the failed fuel rod. In the failed fuel rod, the oxide layer represented 10 μm of the boundary of the cladding and 35 μm of the region outside the cladding. By comparison, in the sound fuel rod, Oxide layer size was 8 μm, which was observed in the cladding boundary region. Zirconium exists in the bonding layer of the (U, Zr)O compound beyond the PCI gap of 20 μm, and oxygen also shows the tendency of zirconium in the failed fuel rod. The composition of U, Zr, and O in the bonding layer of the failed fuel was 12.87 at.%, 25.76 at.%, and 61.36 at.%, respectively. Its chemical formula can be written as UZr_2O_3 [13].

The status of the fission products in the recoil area was analyzed using an EPMA. The significance of the analysis means that it is possible to measure the fission distribution of the recoil layer region using SIMS and EPMA instruments. The results of this study can be used in the consideration of interim storage facilities for spent fuels used in Korean nuclear power plants.

References

1. J. Julien, I. Z-Aubrun, J. Sercombe, G. Raveu, and J. M. Gatt, *Proc. Top Fuel 2012*, p. 96, European Nuclear Society, Manchester, UK (2012).
2. B. Cox, *J. Nucl. Mater.*, **172**, 249 (1990).
3. A. Denis and A. Soba, *J. Nucl. Eng. Des.*, **223**, 211 (2003).
4. N. Marchal, C. Campos, and C. Garnier, *Comput. Mater. Sci.*, **45**, 821 (2009).
5. H. Kleykamp, *J. Nucl. Mater.*, **131**, 230 (1985).
6. R. Restani, E. T. Aerne, G. Bart, H. P. Linder, A. Müller, and F. Petrik, Characterisation of PWR Cladding Hulls from Commercial Reprocessing, Technical Reprot NTB-92-13, Nagra, Swizerland (1992).
7. Y. H. Jung, K. H. Kang, I. H. Jung, J. M. Park, G. S. Kim, Y. S. Choo, K. C. Song, and K. P. Hong, *J. Nucl. Mater.*, **377**, 444 (2008).
8. Y.-k Ha, Chemical interaction between UO_2 fuel and Zircaloy clad, KAERI/AR-697 (2004).
9. K. Maeda, The measurement and evaluation of fuel cladding chemical interaction between Fuels and cladding materials, *KAERI-JAEA Experts Meeting* (2010).
10. Y. Nishino, A. R. Krauss, Y. Lin, and D. M. Gruen, *J. Nucl. Mater.*, **228**, 346 (1996).
11. D. J. Park, J. Y. Park, and Y. H. Jeong, *J. Nucl. Mater.*, **412**, 233 (2011).
12. H. C. Suk, K.-S. Sim, and J. H. Park, *J. Nucl. Eng. Des.*, **165**, 81 (1996).
13. Y. H. Jung, S. J. Baik, Y. G. Jin, and S. B. Ahn, *Proc. KNS Spring Meeting*, Jeju, Korea (2019).